Adjusting amplitude of the stored optical solitons by inter-dot tunneling coupling in triple quantum dot molecules

Yin Wang(王胤)[1,†], Si-Jie Zhou(周驷杰)[2], Yong-He Deng(邓永和)[1], and Qiao Chen(陈桥)[1]

[1] *School of Computational Science and Electronics, Hunan Institute of Engineering, Xiangtan* 411104, *China*
[2] *Department of Physics, Xiangtan University, Xiangtan* 411105, *China*

(Received 7 June 2022; revised manuscript received 19 August 2022; accepted manuscript online 5 September 2022)

We study the propagation properties of a probe field in an aligned asymmetric triple quantum dot molecule with both sides inter-dot tunneling coupling effect. It is shown that the probe field can form optical soliton due to the destructive quantum interference induced by the quantum inter-dot tunneling coupling effect. Interestingly, these optical solitons can be stored and retrieved by adjusting single or double inter-dot tunneling coupling effect, different from that light memory in the ultra-cold atom system. Furthermore, we also find that the amplitude of the stored optical soliton can be adjusted by the strength of the single or double inter-dot tunneling coupling. It is possible to improve the stability and the fidelity of the optical information in the process of the storage and retrieval in semiconductor quantum dots devices.

Keywords: tunneling induced transparency, triple quantum dot molecules, the storage and retrieval of the optical solitons

PACS: 42.50.Gy, 42.65.Tg, 78.67.Hc **DOI:** 10.1088/1674-1056/ac8f3d

1. Introduction

Quantum information is easily transmitted by lights, however the lights need to be stored locally to process the information.[1,2] Fleischhauer and Lukin[3] confirmed that the probe field can be stored by switching off and on control field in the ultra-cold atomic electromagnetically induced transparency (EIT) media. So, it's quite beneficial for the storage and retrieval of the quantum information.[4–10] However, in the process of the storage and retrieval of the light propagation, the diffraction and dispersion effect of light bring about distortion of quantum information in some degree. Comparing with light, the optical solitons,[11] which are from the nonlinear effect of the system being balanced with the diffraction (dispersion) effect, have higher stability and fidelity, and have gained considerable attention in ultra-cold atomic EIT media.[12–18]

For the ultra-cold atomic EIT media, the storage and retrieval properties of the probe field in ladder-type three-level atomic system was firstly investigated.[19] Due to the existence of the dark state,[3] the control field can control the probe field to realize storage and retrieval of the probe optical solitons.[19,20] In reality, there is a lot of information coexisting in quantum information processing and transmission. Correspondingly, the storage and retrieval of two-component even N-component optical solitons are considered and investigated.[21,22] Furthermore, by considering the optical quantum memory, Chen *et al.*[23] found that the high-dimensional light pulses can also be stored and retrieved by switching off and on a control field. For the practical application, however, it is a large challenge to control accurately the optical solitons storage in the atomic EIT media due to its low temperature (which approaches to absolute zero) and rarefaction.

Fortunately, with the maturity of semiconductor quantum technology, quantum dots (QDs) have extensively applying prospect in quantum information processing and transmission.[24,25] This is mainly because the QDs have not only similar optical properties to atomic system, but also the characteristics of high nonlinear optical coefficient, controllable parameters and easy integration.[26–28] Thereby, the studies on the quantum information processing and transmission of quantum dot systems have begun to attract ones' attention.[29–35] In general, two and more QDs, of which inter-dot couplings are realized by placing a gate electrode experimentally, are called as double quantum dot (QD) and multi-quantum dot molecules, respectively. For the double QD molecules, the quantum destructive interference caused by inter-dot tunneling coupling leads to the transparency of the medium, which is called as quantum inter-dot tunneling induced transparency (TIT).[36,37] This is similar to the EIT effect in a three-level ultra-cold atomic medium. She *et al.*[38] studied the linear optical and Kerr nonlinear properties of double QD system. They found that there exist two transparent windows and the type of the optical soliton can also be controlled by changing the intensity of the control field.[38] Experimentally, the triple quantum dot (TQD) molecules have been obtained by molecular beam epitaxy or *in-situ* atomic layer precision etching schemes.[39–42] Compared with the double quantum dot system, the TQD system has more flexible and controllable geometry configuration and extra control parameters. Especially, the TQD molecules possess double quantum

[†]Corresponding author. E-mail: 21112@hnie.edu.cn

© 2023 Chinese Physical Society and IOP Publishing Ltd

inter-dot tunneling coupling effect. After the double quantum inter-dot tunneling couplings are considered, the nonlinear response of the system is enhanced largely.[43,44] Luo *et al.*[45,46] also confirmed that the Kerr nonlinearity of the TQD system can dramatically be enhanced compared to that of double QD system. This means that there exhibit a series of novel nonlinear properties in TQD molecule device. We[47] found that the propagating velocity of the optical soliton can be controlled by the two tunneling coupling strengths. To our knowledge, there are few reports on the storage and retrieval of optical solitons in the QD systems by far.

Inspired by this, in the paper, we study how both sides inter-dot tunneling control the propagation of optical field in an aligned asymmetric TQD molecular model. Especially, we demonstrate that optical solitons can be stored and retrieved by switching off and on single (two) quantum inter-dot tunneling coupling effect. That is to say, both the formation of optical solitons and their storage and retrieval in an TQD molecule are caused by inter-dot tunneling coupling effect, different with that by the strong control optical field in ultra-cold atomic EIT media. Our scheme avoids the noise problem because the system has only one probe field.[27,48,49] The threshold power ($\bar{P}_{\max}$) for generating optical solitons is extremely low, that is, about $\bar{P}_{\max} \approx 2.37\times10^{-7}$ W. Such a low power can enhance the nonlinearity of the system, which is mainly due to the double TIT caused by the two inter-dot tunneling coupling. Additionally, in the case that one (the another) inter-dot tunneling coupling is turned on (off), with the increasing strength of the inter-dot tunneling coupling, the amplitude of the stored optical soliton increases monotonously. For the case that two inter-dot tunneling coupling are turned on, with the increasing strength of the two inter-dot tunneling coupling, the amplitude of the stored optical soliton emerges a trend of first decreasing and then increasing. Our results may improve the stability and fidelity for the storage and retrieval of optical information in semiconductor quantum dot devices.

2. The Maxwell–Bloch equations and asymptotic expansion

2.1. The model

Based on the current experiment reports on quantum dot molecules,[39–42] triple QD system can be produced on the n^+-doped GaAs (001) substrate by molecule beam epitaxy or in-situ atomic layer precise etching, and thus enables a homogeneous triple QD aligned along the $[1\bar{1}0]$ direction. We here consider a self-assembled GaAs TQD molecular system as shown in Fig. 1(a). Among them, a weak probe laser filed with the frequency ω_p is nearly resonant with the direct excitonic transition $|1\rangle \leftrightarrow |4\rangle$. The three QD are aligned, and their sizes appear different, so that the system is an asymmetric TQD molecule. We consider a structural asymmetry, which is to inhibit the hole tunneling. Both QD2 and QD3 are coupled to QD1 by inter-dot tunneling coupling, of which the strength are T_{e1} and T_{e2}, respectively. Such a phenomenon can be realized by applied gate voltages in the experiment. Without the gate voltage, the conduction-band levels are out of resonance and the electron tunneling is very weak. On the contrary, after the gate voltages are applied, as shown in Fig. 1(b), conduction-band levels could get closer to resonance and the electron tunneling between the QDs becomes strong, while valance-band levels become even more off-resonance.

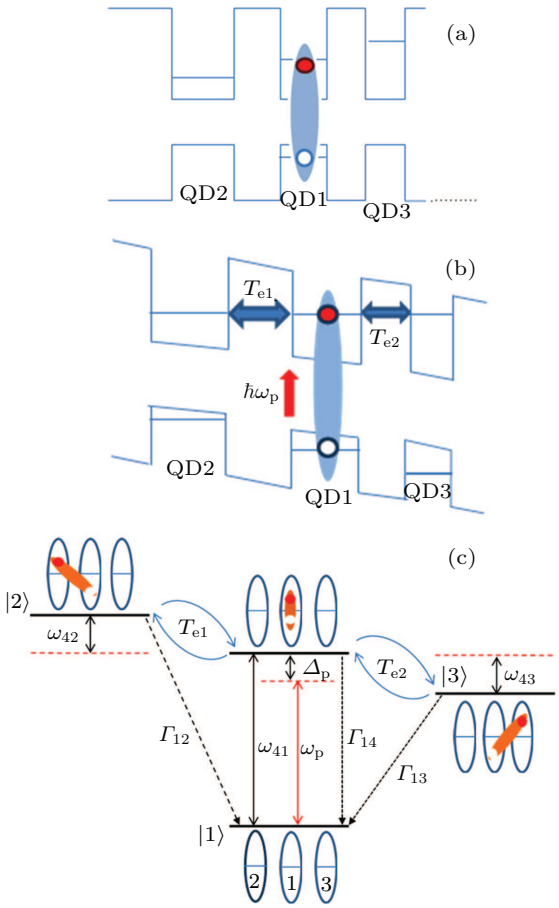


Fig. 1. (a) Schematic diagram of an aligned asymmetric TQD system without gate voltage. An optical field transmits in QD1. (b) When gate voltages are applied respectively between QD1 with QD2, and QD1 with QD3, the conduction-band levels could get closer to resonance. T_{e1} and T_{e2} are the strength of inter-dot tunneling coupling of between QD1 with QD2, and QD1 with QD3, respectively. (c) The excitation scheme of the TQD system. $|1\rangle$ is the exciton vacuum state, which denotes that there are no excitons inside the TQD. Under the excitation of the optical field, electrons are excited from the valence band to the conduction band, forming a direct exciton state $|4\rangle$ in QD1. Due to that the gate voltages are applied, electrons tunnel from QD1 to QD2 or QD3, forming indirect exciton states $|2\rangle$ or $|3\rangle$, respectively. ω_{4m} ($m = 1, 2, 3$) denotes the energy-level difference between $|4\rangle$ and $|m\rangle$. $\Delta_p = \omega_p - \omega_{41}$ represents the detuning of the optical field. Γ_{1n} ($n = 2, 3, 4$) are the energy relaxation rates from state $|n\rangle$ to state $|1\rangle$.

As shown in Fig. 1(c), without the optical field excitation, there is no electron and hole inside all QDs, and this condition can be described by the exciton vacuum state $|1\rangle$. Applying the optical field, one can excite an electron–hole pair

in QD1, which corresponds to the direct exciton state $|4\rangle$. We set the optical field to propagate along the z direction. Then, the electric field vector of the optical field can be written as $\boldsymbol{E} = \boldsymbol{e}_{\rm p}\mathcal{E}_{\rm p}\exp\left[{\rm i}(\boldsymbol{k}_{\rm p}\cdot\boldsymbol{z} - \omega_{\rm p}t)\right] + {\rm c.c.}$ Here, $\boldsymbol{e}_{\rm p}$ is the polarization direction of the optical field, $\mathcal{E}_{\rm p}$ is the envelope amplitude of the optical field, and $\boldsymbol{k}_{\rm p}$ is the wave number of the optical field. The external electric fields modify the band profiles alignment, allowing the electron to tunnel from QD1 to QD2 or QD3 that form the indirect exciton states $|2\rangle$ or $|3\rangle$, respectively.

Under electric-dipole and rotating-wave approximation, the Hamiltonian of the system, in the interaction picture, is

$$\begin{aligned} H_{\rm int} =& -\hbar\Delta_2|2\rangle\langle 2| - \hbar\Delta_3|3\rangle\langle 3| - \hbar\Delta_{\rm p}|4\rangle\langle 4| \\ & -\hbar(\Omega_{\rm p}|4\rangle\langle 1| + T_{\rm e1}|4\rangle\langle 2| + T_{\rm e2}|4\rangle\langle 3| + {\rm h.c.}), \end{aligned} \tag{1}$$

where h.c. represents the Hermitian conjugation. Here $\Delta_{\rm p} = \omega_{\rm p} - \omega_{41}$ denotes the detuning of the optical field, and $\Delta_{2(12)} = \Delta_{\rm p} + \omega_{42(43)}$, with $\omega_{42(43)}$ denoting the frequency difference between state $|4\rangle$ and state $|2\rangle$ ($|3\rangle$). Experimentally, $\omega_{42(43)}$ can be modulated by applying a gate field F along the growth direction, leading to the energy-level shift $\Delta\omega_{42(43)} = eFd$, with d being the width of the barrier between the neighboring dots.[46,50,51] The half-Rabi frequency of the optical field is $\Omega_{\rm p} = \mathcal{E}_{\rm p}P_{14}/(2\hbar)$, with P_{14} the electric dipole matrix element related with the transition between $|1\rangle$ and $|4\rangle$. $T_{\rm e1}$ and $T_{\rm e2}$ are corresponding inter-dot tunneling strengths of between QD1 with QD2 and QD1 with QD3, respectively.

Then, the semi-classical theory is used to solve the physical properties of the system. For the quantum dots, the Bloch equation of quantum mechanics is adopted. Accordingly, the density matrix elements of Bloch equations, in the interaction picture, read

$$\frac{\partial\rho_{11}}{\partial t} = {\rm i}\Omega_{\rm p}^*\rho_{41} - {\rm i}\Omega_{\rm p}\rho_{41}^* + \Gamma_{12}\rho_{22} + \Gamma_{13}\rho_{33} + \Gamma_{14}\rho_{44}, \tag{2a}$$

$$\frac{\partial\rho_{22}}{\partial t} = {\rm i}T_{\rm e1}\rho_{42} - {\rm i}T_{\rm e1}\rho_{42}^* - \Gamma_{12}\rho_{22}, \tag{2b}$$

$$\frac{\partial\rho_{33}}{\partial t} = {\rm i}T_{\rm e2}\rho_{43} - {\rm i}T_{\rm e2}\rho_{43}^* - \Gamma_{13}\rho_{33}, \tag{2c}$$

$$\begin{aligned} \frac{\partial\rho_{44}}{\partial t} =& {\rm i}\Omega_{\rm p}\rho_{41}^* + {\rm i}T_{\rm e1}\rho_{42}^* + {\rm i}T_{\rm e2}\rho_{43}^* - {\rm i}\Omega_{\rm p}^*\rho_{41} \\ & - {\rm i}T_{\rm e1}\rho_{42} - {\rm i}T_{\rm e2}\rho_{43} - \Gamma_{14}\rho_{44}, \end{aligned} \tag{2d}$$

$$\frac{\partial\rho_{21}}{\partial t} = {\rm i}\Delta_2\rho_{21} + {\rm i}T_{\rm e1}\rho_{41} - {\rm i}\Omega_{\rm p}\rho_{42}^* - \gamma_{21}\rho_{21}, \tag{2e}$$

$$\frac{\partial\rho_{31}}{\partial t} = {\rm i}\Delta_3\rho_{31} + {\rm i}T_{\rm e2}\rho_{41} - {\rm i}\Omega_{\rm p}\rho_{43}^* - \gamma_{31}\rho_{31}, \tag{2f}$$

$$\begin{aligned} \frac{\partial\rho_{32}}{\partial t} =& {\rm i}\Delta_3\rho_{32} + {\rm i}T_{\rm e2}\rho_{42} - {\rm i}\Delta_2\rho_{32} \\ & - {\rm i}T_{\rm e1}\rho_{43}^* - \gamma_{32}\rho_{32}, \end{aligned} \tag{2g}$$

$$\begin{aligned} \frac{\partial\rho_{41}}{\partial t} =& {\rm i}\Omega_{\rm p}\rho_{11} + {\rm i}T_{\rm e1}\rho_{21} + {\rm i}T_{\rm e2}\rho_{31} \\ & + {\rm i}\Delta_{\rm p}\rho_{41} - {\rm i}\Omega_{\rm p}\rho_{44} - \gamma_{41}\rho_{41}, \end{aligned} \tag{2h}$$

$$\begin{aligned} \frac{\partial\rho_{42}}{\partial t} =& {\rm i}\Omega_{\rm p}\rho_{21}^* + {\rm i}T_{\rm e1}\rho_{22} + {\rm i}T_{\rm e2}\rho_{32} + {\rm i}\Delta_{\rm p}\rho_{42} \\ & - {\rm i}\Delta_2\rho_{42} - {\rm i}T_{\rm e1}\rho_{44} - \gamma_{42}\rho_{42}, \end{aligned} \tag{2i}$$

$$\begin{aligned} \frac{\partial\rho_{43}}{\partial t} =& {\rm i}\Omega_{\rm p}\rho_{31}^* + {\rm i}T_{\rm e1}\rho_{32}^* + {\rm i}T_{\rm e2}\rho_{33} + {\rm i}\Delta_{\rm p}\rho_{43} \\ & - {\rm i}\Delta_3\rho_{43} - {\rm i}T_{\rm e2}\rho_{44} - \gamma_{43}\rho_{43}, \end{aligned} \tag{2j}$$

where $\gamma_{ij} = (\Gamma_i + \Gamma_j)/2$ denotes the coherence decay rate between state $|i\rangle$ and state $|j\rangle$, with $\Gamma_j = \sum_{i<j}\Gamma_{ij}$ being the total decay rate of state $|j\rangle$. Γ_{ij} are the energy relaxation rates from state $|j\rangle$ to state $|i\rangle$. For simplicity, here we do not consider effects of pure dephasing.[39,44]

For the light field, the classical Maxwell equation is used. Under a slowly varying envelope approximation, the evolution equation of the classical Maxwell[14,52] is

$${\rm i}\left(\frac{\partial}{\partial z} + \frac{1}{c}\frac{\partial}{\partial t}\right)\Omega_{\rm p} + \kappa_{14}\rho_{41} = 0, \tag{3}$$

where $\kappa_{14} = N\omega_{\rm p}|\boldsymbol{P}_{14}|^2/(2\varepsilon_0 c\hbar)$ is the propagation coefficient, ε_0 is the permittivity of vacuum, and N denotes the atomic concentration. Thereby, only if solving Maxwell–Bloch (M-B) Eqs. (2) and (3), the linear and nonlinear properties of the system can be well obtained.

2.2. Linear properties

In general, the analytic solution of the M-B Eqs. (2) and (3) cannot be obtained directly. To explore the linear and nonlinear properties, the multiple-scale method[14] is a good approximation method for solving nonlinear differential equations and is widely used in applied mathematics and physics. Therefore, we make the asymptotic expansion $\rho_{ij} = \rho_{ij}^{(0)} + \varepsilon\rho_{ij}^{(1)} + \varepsilon^2\rho_{ij}^{(2)} + \varepsilon^3\rho_{ij}^{(12)} + \cdots$, and $\Omega_{\rm p} = \varepsilon\Omega_{\rm p}^{(1)} + \varepsilon^2\Omega_{\rm p}^{(2)} + \varepsilon^3\Omega_{\rm p}^{(3)} + \cdots$. Here, $\rho_{ij}^{(0)} = \delta_{i1}\delta_{j1}$ means the electron population, which was concentrated at the ground state $|1\rangle$ with the first time, and ε is a dimensionless small parameter characterizing the amplitude of $\Omega_{\rm p}$. At the same time, we set that the expansion terms are functions of the multiscale variables $z_l = \varepsilon^l z$ ($l = 0,1,2$) and $t_l = \varepsilon^l t$ ($l = 0,1$). Subsequently, substituting them into the M-B equations and comparing the coefficients of ε^l ($l = 1,2,3,\ldots$), we obtain the first-order solution

$$\Omega_{\rm p}^{(1)} = F\,{\rm e}^{{\rm i}\theta}, \tag{4a}$$

$$\rho_{41}^{(1)} = \frac{F\,{\rm e}^{{\rm i}\theta}(d_{21}+\omega)(d_{31}+\omega)}{D(\omega)}, \tag{4b}$$

$$\rho_{21}^{(1)} = \frac{-T_{\rm e1}}{d_{21}+\omega}\rho_{41}^{(1)}, \tag{4c}$$

$$\rho_{31}^{(1)} = \frac{-T_{\rm e2}}{d_{31}+\omega}\rho_{41}^{(1)}, \tag{4d}$$

with other $\rho_{ij}^{(1)} = 0$. Here $D(\omega) = T_{\rm e1}^2(d_{31}+\omega) + T_{\rm e2}^2(d_{21}+\omega) - (d_{21}+\omega)(d_{31}+\omega)(d_{41}+\omega)$, $\theta = K(\omega)z_0 - \omega t_0$, $d_{21} = \Delta_2 + {\rm i}\gamma_{21}$, $d_{31} = \Delta_3 + {\rm i}\gamma_{31}$, and $d_{41} = \Delta_{\rm p} + {\rm i}\gamma_{41}$. F

is the envelope function of the variables z_1, z_2, t_1. Meanwhile, we obtain that the linear dispersion relation $K(\omega)$ is

$$K(\omega)=\frac{\omega}{c}+\kappa_{14}\frac{(d_{21}+\omega)(d_{31}+\omega)}{D(\omega)}. \tag{5}$$

In most case, by applying the Taylor expansion, $K(\omega)$ can be expressed as $K(\omega)=K_0+K_1\omega+\frac{1}{2}K_2\omega^2+\cdots$ with $K_j=\left(\partial^j K(\omega)/\partial\omega^j\right)\big|_{\omega=0}$ $(j=0,1,2,\ldots)$. Due to K_j is a complex number, it can be written as $K_j=K_{j\mathrm{r}}+\mathrm{i}K_{j\mathrm{i}}$. So $K_{0\mathrm{r}}$, $K_{1\mathrm{r}}$ and $K_{2\mathrm{r}}$ represent the real parts of K_0, K_1 and K_2, respectively. Similarly, $K_{0\mathrm{i}}$, $K_{1\mathrm{i}}$ and $K_{2\mathrm{i}}$ represent the imaginary parts of K_0, K_1 and K_2, respectively. In fact, $K_{0\mathrm{i}}$ determines the linear absorption of the probe field. In order to obtain the linear absorption properties of the optical field in the system, we plot $K_{0\mathrm{i}}$ as a function of the Δ_p shown in Fig. 2. From Fig. 2(a), when the two inter-dot tunneling coupling are absent, i.e., $T_{\mathrm{e}1}=T_{\mathrm{e}2}=0$ [see the black dotted curve in Fig. 2(a)], there only appears a Lorentz line-shape absorption peak. This means that when the gate voltage is turned off, the optical field is largely absorbed in the area of its detuning. When the gate voltage between QD1 with QD2 (QD1 with QD3) is turned off (on), i.e., $T_{\mathrm{e}1}=0$ and $T_{\mathrm{e}2}=20$ μeV [see the red solid curve in Fig. 2(a)], the absorption profile is split into two separate peaks, and the single quantum inter-dot TIT window appears in the system. Due to that the optical field is hardly absorbed in the quantum inter-dot TIT window, in the following, we will study the nonlinear properties in the area of the transparent window. When the single inter-dot tunneling coupling $T_{\mathrm{e}2}$ is enhanced, i.e., $T_{\mathrm{e}1}=0$ and $T_{\mathrm{e}2}=40$ μeV [see the blue dashed curve in Fig. 2(a)], the width of the quantum inter-dot TIT window becomes wider by comparing with the red solid curve. When the gate voltage between QD1 with QD2 (QD1 with QD3) is turned on (off), it is also found that the width of the transparency window increases with the increasing strength of tunneling coupling. Its phenomenon is similar to that in Fig. 2(a). Subsequently, when the two inter-dot tunneling coupling are present, i.e., $T_{\mathrm{e}1}=T_{\mathrm{e}2}=20$ μeV [see the red solid curve in Fig. 2(b)], the double TIT window appears in the system, which is different from the single quantum inter-dot TIT window in double QD molecule. The single (double) TIT window is due to the quantum destructive interference effect induced by single (double) inter-dot tunneling coupling effect, which is different from the EIT window caused by control field in the ultra-cold atomic system. When both tunneling couplings are enhanced, i.e., $T_{\mathrm{e}1}=T_{\mathrm{e}2}=40$ μeV [see the blue dashed curve in Fig. 2(b)], the width of the double TIT windows become wider than that of the red solid curve. In addition, from the red solid curve of Fig. 2(a) [$T_{\mathrm{e}1}=0$, $T_{\mathrm{e}2}=20$ μeV], ones see that the center position of the TIT window is not at $\Delta_\mathrm{p}=0$, which is due to $T_{\mathrm{e}1}\neq T_{\mathrm{e}2}$. Only if $T_{\mathrm{e}1}=T_{\mathrm{e}2}$ [see the Fig. 2(b)], the TIT window exhibits symmetric distribution. The width of both single and/or double quantum inter-dot TIT windows becomes wider with the increasing strength of single and/or double inter-dot tunneling coupling. And in the case of the strength of the double inter-dot tunneling coupling effect being not equal, i.e., $T_{\mathrm{e}1}\neq T_{\mathrm{e}2}$, two TIT windows exhibit asymmetric distribution.

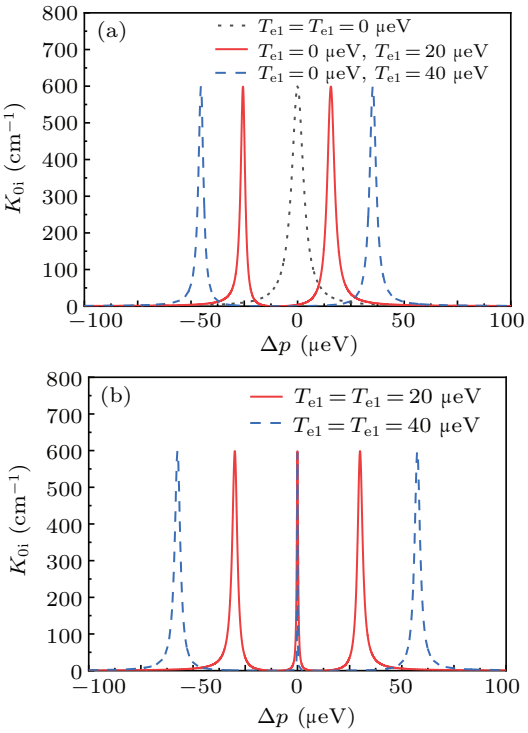


Fig. 2. The linear absorption coefficient $K_{0\mathrm{i}}$ as a function of the detuning Δ_p with different $T_{\mathrm{e}1}$ and $T_{\mathrm{e}2}$. (a) When $T_{\mathrm{e}1}=0$, the black dotted, red solid and blue dashed curve represent $T_{\mathrm{e}2}=0$, $T_{\mathrm{e}2}=20$ μeV and $T_{\mathrm{e}2}=40$ μeV, respectively. (b) The red solid curve and blue dashed curve represent $T_{\mathrm{e}1}=T_{\mathrm{e}2}=20$ μeV and $T_{\mathrm{e}1}=T_{\mathrm{e}2}=40$ μeV, respectively. The other parameters used are $\gamma_{41}=3.3$ μeV, $\gamma_{21}=\gamma_{31}=10^{-4}\gamma_{41}$, $-\hbar\omega_{42}=\hbar\omega_{43}=10$ μeV, $\kappa_{14}=1976$ cm$^{-1}\cdot$μeV.

2.3. Nonlinear properties

Since the linear properties are obtained, we here probe the nonlinear properties of the system, namely, in the case of the second and third order of the M-B equation. For second order, the divergence-free condition requires that

$$\frac{\partial F}{\partial z_1}+\frac{1}{V_\mathrm{g}}\frac{\partial F}{\partial t_1}=0, \tag{6}$$

with $V_\mathrm{g}=(\partial K/\partial\omega)^{-1}$ is the group-velocity of wave packet F. The second order solution is

$$\rho_{41}^{(2)}=\left(K_1-\frac{1}{c}\right)\frac{\mathrm{i}}{\kappa_{14}}\frac{\partial}{\partial t_1}F\,\mathrm{e}^{\mathrm{i}\theta}, \tag{7a}$$

$$\rho_{21}^{(2)}=\left[\frac{T_{\mathrm{e}1}(d_{31}+\omega)}{D(d_{21}+\omega)}-\frac{T_{\mathrm{e}1}}{\kappa_{14}(d_{21}+\omega)}\left(K_1-\frac{1}{c}\right)\right]\times\mathrm{i}\frac{\partial}{\partial t_1}F\,\mathrm{e}^{\mathrm{i}\theta}, \tag{7b}$$

$$\rho_{31}^{(2)}=\left[\frac{T_{\mathrm{e}2}(d_{21}+\omega)}{D(d_{31}+\omega)}-\frac{T_{\mathrm{e}2}}{\kappa_{14}(d_{31}+\omega)}\left(K_1-\frac{1}{c}\right)\right]\times\mathrm{i}\frac{\partial}{\partial t_1}F\,\mathrm{e}^{\mathrm{i}\theta}, \tag{7c}$$

$$\rho_{33}^{(2)} = A_{33}^{(2)}|F|^2 \mathrm{e}^{-2\mathrm{Im}(K)z}, \tag{7d}$$
$$\rho_{22}^{(2)} = A_{22}^{(2)}|F|^2 \mathrm{e}^{-2\mathrm{Im}(K)z}, \tag{7e}$$
$$\rho_{11}^{(2)} = A_{11}^{(2)}|F|^2 \mathrm{e}^{-2\mathrm{Im}(K)z}, \tag{7f}$$
$$\rho_{42}^{(2)} = A_{42}^{(2)}|F|^2 \mathrm{e}^{-2\mathrm{Im}(K)z}, \tag{7g}$$
$$\rho_{43}^{(2)} = A_{43}^{(2)}|F|^2 \mathrm{e}^{-2\mathrm{Im}(K)z}, \tag{7h}$$
$$\rho_{32}^{(2)} = A_{32}^{(2)}|F|^2 \mathrm{e}^{-2\mathrm{Im}(K)z}, \tag{7i}$$

where the detailed expressions of $A_{33}^{(2)}$, $A_{22}^{(2)}$, $A_{11}^{(2)}$, $A_{42}^{(2)}$, $A_{43}^{(2)}$ and $A_{32}^{(2)}$ are given in the Appendix. Next, for the third order, we have the nonlinear equation for F by the divergence-free condition

$$\mathrm{i}\frac{\partial F}{\partial z_2} - \frac{1}{2}K_2\frac{\partial^2 F}{\partial t_1^2} - WF|F|^2 \mathrm{e}^{-2\mathrm{Im}(K)z} = 0, \tag{8}$$

where K_2 is the group-velocity dispersion coefficient, and $W = \frac{\kappa_{14}(d_{21}+\omega)(d_{31}+\omega)}{D}[T_{e1}A_{42}^{(2)*}/(d_{21}+\omega) + T_{e2}A_{43}^{(2)*}/(d_{31}+\omega) + 2A_{11}^{(2)} + A_{22}^{(2)} + A_{33}^{(2)}$ denotes Kerr nonlinear coefficient.

After returning Eq. (8) to the original variable, we get the nonlinear Schrödinger (NLS) equation

$$\mathrm{i}\frac{\partial U}{\partial z} - \frac{1}{2}K_2\frac{\partial^2 U}{\partial \tau^2} - W|U|^2 U = 0, \tag{9}$$

where $\tau = t - z/V_\mathrm{g}$ and $U = \varepsilon F \mathrm{e}^{-\mathrm{Im}(K)z}$. Due to that the coefficients of the NLS Eq. (9) are complex number, in general, the NLS equation has no analytical soliton solution. So, we here choose appropriate parameters in the area of the transparent window. According to Refs. [35,43] the parameters of the system can be chosen as $\hbar\omega_{41} = 1.6$ μeV, $\Gamma_{14} = 6.6$ μeV, $\Gamma_{12} = \Gamma_{13} = 6.6\times10^{-4}$ μeV, $\gamma_{41} = 3.3$ μeV, $\gamma_{21} = \gamma_{31} = 10^{-4}\gamma_{41}$, $-\hbar\omega_{42} = \hbar\omega_{43} = 10$ μeV and $\kappa_{14} = 1976\ \mathrm{cm}^{-1}\cdot$μeV. When $T_{e1} = T_{e2} = 7.5\times10^{10}\ \mathrm{s}^{-1} \approx 50$ μeV and $\Delta_\mathrm{p} = 1.516\times10^{10}\ \mathrm{s}^{-1}$, we obtain

$$K_0 = (-0.013 + 2.680\times10^{-4}\mathrm{i})\ \mathrm{cm}^{-1},$$
$$K_1 = (5.675\times10^{-10} + 4.003\times10^{-14}\mathrm{i})\ \mathrm{cm}^{-1}\cdot\mathrm{s},$$
$$K_2 = (-3.242\times10^{-20} + 9.580\times10^{-22}\mathrm{i})\ \mathrm{cm}^{-1}\cdot\mathrm{s}^2,$$
$$W = (-7.102\times10^{-13} - 4.974\times10^{-15}\mathrm{i})\ \mathrm{cm}^{-1}\cdot\mathrm{s}^2.$$

One may see that $|K_{2\mathrm{i}}| \ll |K_{2\mathrm{r}}|$ and $|W_\mathrm{i}| \ll |W_\mathrm{r}|$, so that $K_2 = K_{2\mathrm{r}} + K_{2\mathrm{i}} \approx K_{2\mathrm{r}}$ and $W = W_\mathrm{r} + W_\mathrm{i} \approx W_\mathrm{r}$. Thereby, Eq. (9) in the dimensionless case is transformed into

$$\mathrm{i}\frac{\partial u}{\partial \zeta} + \frac{\partial^2 u}{\partial \sigma^2} + 2|u|^2 u = 0, \tag{10}$$

where the dimensionless parameters $\zeta = -z/2L_\mathrm{D}$, $\sigma = \tau/\tau_0$ and $u = U/U_0$. Here τ_0 is the characteristic optical field length. $U_0 \equiv \sqrt{|K_{2\mathrm{r}}|}/|W_\mathrm{r}|/\tau_0$ is the Rabi frequency of the optical field, and its magnitude depends on the initial value. In addition, we introduce $L_\mathrm{D} = \tau_0^2/|K_{2\mathrm{r}}|$ and $L_\mathrm{NL} = 1/(|W_\mathrm{r}|U_0^2|)$. Here, L_D and L_NL represent the dispersion and nonlinear length, respectively. According to the condition of soliton formation, i.e., $L_\mathrm{D} = L_\mathrm{NL}$, this means the balance of the interplay between the group-velocity dispersion and nonlinear effect. Equation (10) has a simple bright soliton solution $u = \mathrm{sech}(\sigma)\exp(\mathrm{i}\zeta)$, which is written in terms of the optical field as

$$\Omega_\mathrm{p}(z,t) = \frac{1}{\tau_0}\sqrt{\frac{K_{2\mathrm{r}}}{W_\mathrm{r}}}\,\mathrm{sech}\left[\frac{1}{\tau_0}\left(t - \frac{z}{V_\mathrm{g}}\right)\right] \times \exp\left[\mathrm{i}K_{0\mathrm{r}}z - \mathrm{i}\frac{z}{2L_\mathrm{D}}\right]. \tag{11}$$

In order to test the stability of the optical soliton in the process of propagation, we plot the wave shape $|\Omega_\mathrm{p}/U_0|^2$ of the bright optical soliton as a function of z/L_D and t/τ_0 in Fig. 3. Ones can see that with the evolution of time and distance, the amplitude, width and velocity of the optical soliton keep unchange, hence the optical soliton is robust in the propagation process.

Subsequently, we calculate the optical power density threshold $\bar{P}_\mathrm{max}$ of generating optical solitons by Poynting's vector[14]

$$\bar{P}_\mathrm{max} = 2\varepsilon_0 c n_\mathrm{p} S_0 (\hbar/P_{14})^2 K_{2\mathrm{r}}/(W_\mathrm{r}\tau_0^2). \tag{12}$$

Here, $P_{14}/\mathrm{e} = 2.1$ nm, and $n_\mathrm{p} = 1 + cK_0/\omega_\mathrm{p}$ is the refractive index. The cross-sectional area of the optical field takes the value $S_0 = 1\times10^{-2}\ \mathrm{cm}^2$, and we can calculate that $\bar{P}_\mathrm{max} \approx 2.37\times10^{-7}$ W. Thus, the very low input power is needed for generating optical solitons in this TQD system. Such a low power can enhance the nonlinearity of the system, which is mainly due to the double TIT caused by the two inter-dot tunneling coupling.

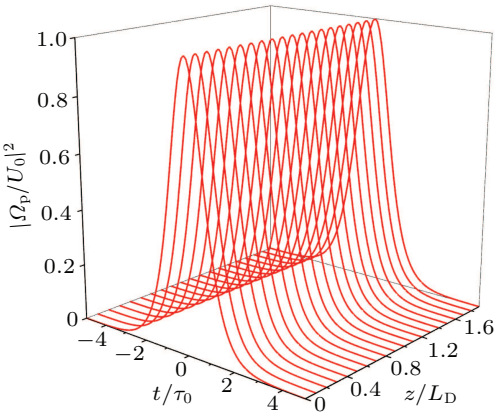


Fig. 3. The propagation of the bright soliton. Wave shape $|\Omega_\mathrm{p}/U_0|^2$ of the optical soliton as a function of z/L_D and t/τ_0.

3. Storage and retrieval of the optical field

Since the optical soliton can propagate steadily, we here explore whether it can be stored and retrieved. Using Runge–Kutta method, we simulate numerically the M-B equations. In order to realize the memory, it is needed to control the two quantum inter-dot tunneling coupling effects. Their switching off and on is modeled by two combined hyperbolic tangent

functions

$$T_{e1}(t) = T_{e10}\left\{1-\frac{1}{2}\tanh\left[\frac{t-T_{off}}{T_s}\right]+\frac{1}{2}\tanh\left[\frac{t+T_{on}}{T_s}\right]\right\}, \tag{13a}$$

$$T_{e2}(t) = T_{e20}\left\{1-\frac{1}{2}\tanh\left[\frac{t-T_{off}}{T_s}\right]+\frac{1}{2}\tanh\left[\frac{t+T_{on}}{T_s}\right]\right\}, \tag{13b}$$

where T_{e10} and T_{e20} are constants. T_{on} and T_{off} are switching-on and switching-off, respectively. T_s is the approximate time of switching.

3.1. Double inter-dot tunneling coupling case

The initial condition of the optical field can be chosen as the hyperbolic secant function, $\Omega_p(0,t) = \Omega_{p0}\,\mathrm{sech}(t/\tau_0)$. To obtain the storage and retrieval of optical field under different cases, we plot the optical field evolution of $|\Omega_p\tau_0|$ and $|T_{e1(2)}\tau_0|$ as a function of time t with different propagation distance z for different input light intensities Ω_{p0} in the Fig. 4. The parameters used are $\tau_0 = 1\times10^{-9}$ s, $T_{e10} = T_{e20} = 7.5\times10^{10}\ \mathrm{s}^{-1} \approx 50\ \mu\mathrm{eV}$, $T_{e10}\tau_0 = T_{e20}\tau_0 = 75$, $\kappa_{14}\tau_0 \approx 3\times10^3\ \mathrm{cm}^{-1}$, $T_s/\tau_0 = 0.2$, $T_{off}/\tau_0 = 5$ and $T_{on}/\tau_0 = 10$.

Figure 4(a) shows the storage and retrieval of a weak (i.e., linear) optical field. In this case, the dispersion effect of the system is not balanced with the nonlinear effect, in which the dispersion effect is dominant. Although the storage and retrieval of optical field can be realized, the wave shape will widen gradually with the evolution of t and z, which will lead to the distortion of information. This leads to loss of information in quantum information processing and transmission and is not suitable for practical application.

Figure 4(b) shows the storage and retrieval of an optical soliton. In this case, the dispersion and nonlinear effects of the system are balanced. Firstly, the optical field evolves into optical soliton before the storage. Then, the optical soliton is stored in the TQD medium. Finally, the optical soliton is retrieved after the storage. We found that the wave shape of soliton before storage and after retrieval are almost the same. It is proved that storage and retrieval by optical soliton have high fidelity in quantum information processing and transmission.

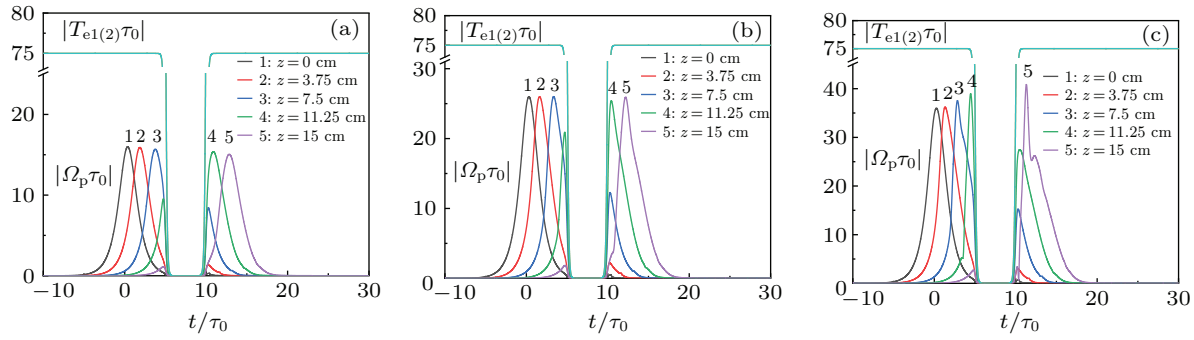


Fig. 4. Storage and retrieval of optical field. (a) Storage and retrieval of a weak optical field, with $\Omega_p(0,t) = 16\mathrm{sech}(t/\tau_0)$. (b) Storage and retrieval of an optical soliton, with $\Omega_p(0,t) = 26\mathrm{sech}(t/\tau_0)$. (c) Storage and retrieval of a strong optical field, with $\Omega_p(0,t) = 36\mathrm{sech}(t/\tau_0)$. $|T_{e1}\tau_0|$ and $|T_{e2}\tau_0|$ represent the switching off and on of the two quantum inter-dot tunneling coupling effects, respectively.

Figure 4(c) shows the storage and retrieval of a strong optical field. In this case, the dispersion effect and the nonlinear effect of the system are not in balance, in which the nonlinear effect is dominant. Comparing the wave shape of the optical field before storage and after retrieval, we can see that the wave shape of the optical field has undergone obvious deformation and even generated some new peaks. This also leads to the loss of information and is not suitable for practical applications.

We here may conclude that optical soliton has better storage and retrieval performance than linear optical field and strongly nonlinear optical field. Therefore, optical soliton has more practical application value than the other two in quantum information processing and transmission. One may ask the question how the optical soliton is stored in the TQD system when both the probe field and the quantum inter-dot tunneling coupling strength have a vanishing value. In fact, in the process of the light storage, the probe-field energy is converted into the energy level coherence of the quantum inter-dot.[53] That is, the probe light is stored in the form of energy level coherence between quantum dots. For our original physical model (1), when the inter-dot tunneling coupling effect T_{e1} (T_{e2}) (which can be realized by applying the applied gate voltages experimentally) is switched off and is retained until the T_{e1} (T_{e2}) is switched on again, the energy level coherence ρ_{12} (ρ_{13}) of the quantum inter-dot can be taken as the intermediary for the storage and retrieval of the probe pulse.

Since the storage and retrieval of optical soliton can be controlled by two inter-dot tunneling coupling effect, we further explore how the strength of two inter-dot tunneling coupling adjust the amplitude of the stored optical soliton. We plot the amplitude of optical soliton as a function of two inter-dot tunneling strengths in Fig. 5. At $\Delta_p = 1.516\times10^{10}\ \mathrm{s}^{-1}$, ones can see that the amplitude of the stored optical soliton first decreases and then increases with the increasing strengths

of the two inter-dot tunneling coupling. So, we conclude that the amplitude of the stored optical soliton can be adjusted by the strength of two quantum inter-dot tunneling coupling.

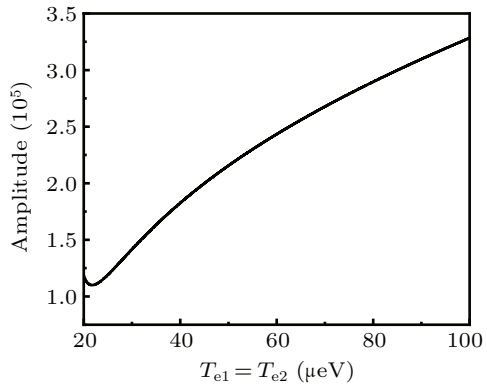


Fig. 5. The amplitude of optical soliton as a function of the strength of two inter-dot tunneling. Both T_{e1} and T_{e2} control the system with $\Delta_p = 1.516 \times 10^{10}$ s^{-1}.

3.2. Single inter-dot tunneling coupling case

Since two quantum inter-dot tunneling coupling effect can control the storage and retrieval of optical soliton, can single quantum inter-dot tunneling coupling effect control the storage and retrieval of optical soliton. In Fig. 6, when T_{e1} is absent and T_{e2} is present, i.e., $T_{e10} = 0$ and $T_{e20} = 6 \times 10^{10}$ s^{-1} ≈ 40 μeV, we plot the evolution of $|\Omega_p \tau_0|$ as a function of time t with different propagation distance z. From Fig. 6, ones can find that the storage and retrieval of optical soliton can be controlled by single quantum inter-dot tunneling coupling strength T_{e2}. Firstly, the optical soliton can be formed based on a single quantum inter-dot TIT effect. Then, the optical soliton is stored in the TQD medium. Finally, the optical soliton can be retrieved after the storage. In another case, when T_{e1} is present and T_{e2} is absent, it is also found that T_{e1} can also control the optical soliton to realize their storage and retrieval.

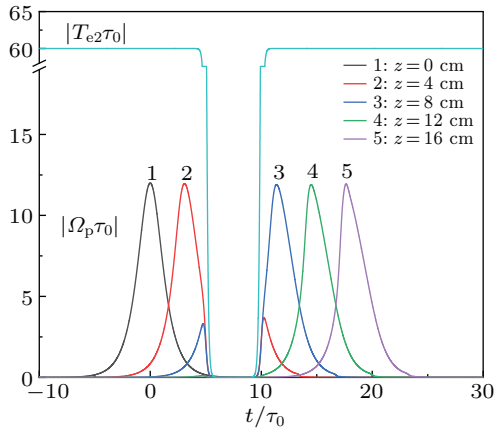


Fig. 6. In case of $T_{e10} = 0$, only T_{e2} controls the storage and retrieval of optical solitons. $\Omega_p(0,t) = 12\,\mathrm{sech}(t/\tau_0)$, $T_{e20} = 6 \times 10^{10}$ s^{-1} $\approx$ 40 μeV. $|T_{e2}\tau_0|$ represents the switching off and on of the tunneling coupling effect which between QD1 with QD3.

Subsequently, we here explore how the strength of single quantum inter-dot tunneling coupling adjust the amplitude of the stored optical soliton. We plot the amplitude of optical soliton as a function of single inter-dot tunneling strength, as shown in Fig. 7. Ones see that the amplitude of the stored optical soliton increases monotonously with the increasing strength of single quantum inter-dot tunneling coupling.

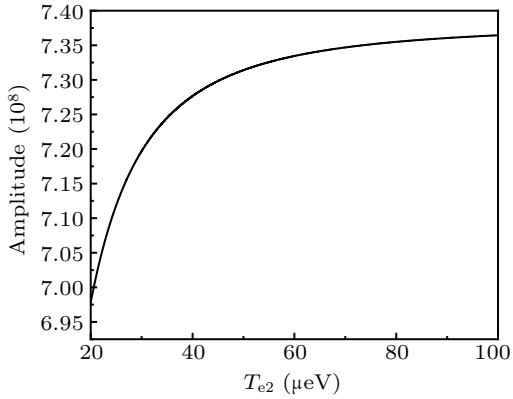


Fig. 7. The amplitude of optical soliton versus the strength of single quantum inter-dot tunneling. Only T_{e2} controls the system with $\Delta_p = -9 \times 10^9$ s^{-1}.

On the basis of discussion above, we conclude that the optical soliton can be stored and retrieved by switching off and on single or two quantum inter-dot tunneling coupling effect, different from that by switching off and on control field in the ultra-cold atomic system. And the amplitude of the stored optical soliton can be adjusted by the strength of single or two quantum inter-dot tunneling coupling.

4. Conclusions

In summary, we have studied the propagation properties of optical field in an aligned asymmetric TQD molecule with both sides inter-dot tunneling coupling effect. The interaction properties between the optical field and TQD molecule in the system are described by using the semiclassical theory. The physical properties of the optical field are described by Maxwell equation, while the TQD molecule is described by the Bloch equation of quantum dynamics. So, we obtained the M-B equations governing the linear and nonlinear properties of the system. Due to that the analytic solution of the M-B equations, in general, cannot be obtained directly, we apply the multiple-scale method to solve M-B equations. For the linear case, there appears single (double) TIT window caused by single (two) inter-dot tunneling coupling effect, which is completely different from the EIT window caused by control field in ultra-cold atomic system. Meanwhile, we also found that the width of both single and/or double TIT windows becomes wider with the increasing strength of single and/or double inter-dot tunneling coupling.

For the nonlinear case, by choosing appropriate parameters in the area of the TIT window, the stable propagation of soliton can be realized. We calculated that the threshold power of generating optical solitons is extremely low, that about is

2.37×10^{-7} W. Such a low power can enhance the nonlinearity of the system, which is mainly due to the double TIT caused by the two inter-dot tunneling coupling. Especially, we have demonstrated that the storage and retrieval of optical solitons can be controlled by switching off and on single (two) inter-dot tunneling coupling effect, different from that by switching off and on control fields in the ultra-cold atomic system. In addition, we found that the amplitude of the stored optical soliton can be adjusted by the strength of quantum inter-dot tunneling coupling. For the case that one (the another) quantum inter-dot tunneling coupling is turned on (off), the amplitude of optical soliton increases monotonously with the increasing single tunneling strength. For the case that two quantum inter-dot tunneling coupling are turned on, the amplitude of the optical soliton emerges a trend of first decreasing and then increasing with the increasing strengths of the two inter-dot tunneling coupling. The aligned asymmetric TQD structure can provide two tunneling channels and multiple tunable parameters to support the storage and retrieval of optical solitons, so it will be very flexible in practical applications. This work is possible to improve the fidelity for the storage and retrieval of the optical information in semiconductor QD devices.

Appendix A

The detailed expressions of the coefficients of Eq. (7) are

$$
\begin{aligned}
A_{33}^{(2)} &= \frac{-\mathrm{i}I_5 - \mathrm{i}I_8\left(-\frac{d_{21}d_{31}}{D}+\frac{d_{21}^*d_{31}^*}{D^*}\right) - \mathrm{i}I_4I_7\left(-\frac{d_{21}d_{31}}{D}+\frac{d_{21}^*d_{31}^*}{D^*}\right) + \mathrm{i}\frac{I_1I_7}{I_2}}{I_6+I_3I_7},\\
A_{22}^{(2)} &= \mathrm{i}I_3A_{33}^{(2)} + \mathrm{i}I_4\left(-\frac{d_{21}d_{31}}{D}+\frac{d_{21}^*d_{31}^*}{D^*}\right) - \mathrm{i}\frac{I_1}{I_2},\\
A_{11}^{(2)} &= \mathrm{i}\frac{\frac{d_{21}d_{31}}{D}-\frac{d_{21}^*d_{31}^*}{D^*}+(\Gamma_{12}-\Gamma_{14})A_{22}^{(2)}+(\Gamma_{13}-\Gamma_{14})A_{33}^{(2)}}{\Gamma_{14}},\\
A_{42}^{(2)} &= \mathrm{i}\frac{\frac{T_{\mathrm{e}1}T_{\mathrm{e}2}^2d_{21}d_{31}\mathrm{i}}{D}+T_{\mathrm{e}1}T_{\mathrm{e}2}^2d_{32}(A_{11}^{(2)}+A_{22}^{(2)}+2A_{33}^{(2)})}{T_{\mathrm{e}1}^2+d_{32}d_{43}^*} - T_{\mathrm{e}1}d_{32}\left(A_{11}^{(2)}+2A_{22}^{(2)}+A_{33}^{(2)}\right) - \frac{T_{\mathrm{e}1}d_{31}^*d_{32}\mathrm{i}}{D^*}}{\beta^*},\\
A_{43}^{(2)} &= \mathrm{i}\frac{\frac{d_{32}^*T_{\mathrm{e}1}^2T_{\mathrm{e}2}\left(A_{11}^{(2)}+2A_{22}^{(2)}+A_{33}^{(2)}\right)-\mathrm{i}\frac{T_{\mathrm{e}1}d_{31}^*d_{32}^*}{D}}{T_{\mathrm{e}2}^2-d_{32}^*d_{42}^*} - T_{\mathrm{e}2}d_{32}^*\left(A_{11}^{(2)}+A_{22}^{(2)}+2A_{33}^{(2)}\right) - \mathrm{i}\frac{T_{\mathrm{e}2}d_{21}^*d_{32}^*}{D^*}}{\beta^*},\\
A_{32}^{(2)} &= \mathrm{i}\frac{-T_{\mathrm{e}1}A_{43}^{(2)*}-T_{\mathrm{e}2}A_{42}^{(2)}}{d_{32}},
\end{aligned}
$$

where

$$
\begin{aligned}
&d_{32}=\Delta_3-\Delta_2+\mathrm{i}\gamma_{32},\quad d_{42}=\Delta_{\mathrm{p}}-\Delta_2+\mathrm{i}\gamma_{42},\quad d_{43}=\Delta_{\mathrm{p}}-\Delta_3+\mathrm{i}\gamma_{43},\\
&\alpha=d_{32}d_{42}-T_{\mathrm{e}2}^2-\frac{T_{\mathrm{e}1}^2T_{\mathrm{e}2}^2}{T_{\mathrm{e}1}^2+d_{32}d_{43}^*},\quad \beta=d_{32}d_{43}^*+T_{\mathrm{e}1}^2-\frac{T_{\mathrm{e}1}^2T_{\mathrm{e}2}^2}{T_{\mathrm{e}2}^2-d_{32}d_{42}},\\
&I_1=T_{\mathrm{e}1}[\frac{\frac{-T_{\mathrm{e}1}T_{\mathrm{e}2}^2d_{32}d_{21}}{D\left(T_{\mathrm{e}1}^2+d_{32}d_{43}^*\right)}+\frac{T_{\mathrm{e}1}d_{31}^*d_{32}}{D^*}}{\alpha}-\frac{\frac{-T_{\mathrm{e}1}T_{\mathrm{e}2}^2d_{32}^*d_{21}^*}{D^*\left(T_{\mathrm{e}1}^2+d_{32}^*d_{43}\right)}+\frac{T_{\mathrm{e}1}d_{31}d_{32}^*}{D}}{\alpha^*}],\\
&I_2=\frac{\mathrm{i}d_{32}T_{\mathrm{e}1}^2T_{\mathrm{e}2}^2\Gamma_{12}-\mathrm{i}T_{\mathrm{e}1}^2d_{32}(T_{\mathrm{e}1}^2+d_{32}d_{43}^*)(\Gamma_{12}+\Gamma_{14})}{\alpha\Gamma_{14}(T_{\mathrm{e}1}^2+d_{32}d_{43}^*)}-\frac{\mathrm{i}T_{\mathrm{e}1}^2d_{32}^*\Gamma_{12}+\mathrm{i}T_{\mathrm{e}1}^2d_{32}^*\left(\Gamma_{12}+\Gamma_{14}\right)\left(T_{\mathrm{e}1}^2+d_{32}^*d_{43}\right)}{\Gamma_{14}\left(T_{\mathrm{e}1}^2+d_{32}^*d_{43}\right)\alpha^*}-\Gamma_{12},\\
&I_3=-\frac{\mathrm{i}d_{32}T_{\mathrm{e}1}^2T_{\mathrm{e}2}^2\left(\Gamma_{13}+\Gamma_{14}\right)}{\alpha I_2\Gamma_{14}\left(T_{\mathrm{e}1}^2+d_{32}d_{43}^*\right)}+\frac{\mathrm{i}T_{\mathrm{e}1}^2d_{32}\Gamma_{13}}{\alpha I_2\Gamma_{14}}+\frac{\mathrm{i}T_{\mathrm{e}1}^2d_{32}^*\left(\Gamma_{13}+\Gamma_{14}\right)}{I_2\Gamma_{14}\left(T_{\mathrm{e}1}^2+d_{32}^*d_{43}\right)\alpha^*}-\frac{\mathrm{i}\Gamma_{13}d_{32}^*T_{\mathrm{e}1}^2}{I_2\Gamma_{14}\alpha^*},\\
&I_4=\frac{\mathrm{i}d_{32}T_{\mathrm{e}1}^2T_{\mathrm{e}2}^2}{\alpha I_2\Gamma_{14}(T_{\mathrm{e}1}^2+d_{32}d_{43}^*)}-\frac{\mathrm{i}d_{32}T_{\mathrm{e}1}^2}{\alpha I_2\Gamma_{14}}-\frac{\mathrm{i}d_{32}^*T_{\mathrm{e}1}^2}{I_2\Gamma_{14}\left(T_{\mathrm{e}1}^2+d_{32}^*d_{43}\right)\alpha^*}+\frac{\mathrm{i}d_{32}^*T_{\mathrm{e}1}^2}{I_2\Gamma_{14}\alpha^*},\\
&I_5=T_{\mathrm{e}2}\left[\frac{\frac{d_{31}d_{32}T_{\mathrm{e}1}}{D\left(T_{\mathrm{e}2}^2-d_{32}^*d_{42}^*\right)}+\frac{T_{\mathrm{e}2}d_{21}^*d_{32}^*}{D^*}}{\beta^*}-\frac{\frac{d_{31}^*d_{32}T_{\mathrm{e}1}}{\left(T_{\mathrm{e}2}^2-d_{32}^*d_{42}^*\right)D^*}+\frac{T_{\mathrm{e}2}d_{21}d_{32}}{D}}{\beta^*}\right],\\
&I_6=\frac{\mathrm{i}d_{32}^*T_{\mathrm{e}1}^2T_{\mathrm{e}2}^2\Gamma_{13}}{\Gamma_{14}(T_{\mathrm{e}2}^2-d_{32}^*d_{42}^*)\beta^*}-\frac{\mathrm{i}T_{\mathrm{e}2}^2d_{32}^*\left(\Gamma_{13}+\Gamma_{14}\right)}{\Gamma_{14}\beta^*}-\frac{\mathrm{i}d_{32}T_{\mathrm{e}1}^2T_{\mathrm{e}2}^2\Gamma_{13}}{\beta\Gamma_{14}\left(T_{\mathrm{e}2}^2-d_{32}d_{42}\right)}+\frac{\mathrm{i}d_{32}T_{\mathrm{e}2}^2\left(\Gamma_{13}+\Gamma_{14}\right)}{\beta\Gamma_{14}}-\Gamma_{13},\\
&I_7=\frac{\mathrm{i}T_{\mathrm{e}1}^2T_{\mathrm{e}2}^2d_{32}^*(\Gamma_{12}+\Gamma_{14})}{\Gamma_{14}(T_{\mathrm{e}2}^2-d_{32}^*d_{42}^*)\beta^*}-\frac{\mathrm{i}T_{\mathrm{e}2}^2d_{32}^*\Gamma_{12}}{\Gamma_{14}\beta^*}-\frac{\mathrm{i}d_{32}T_{\mathrm{e}1}^2T_{\mathrm{e}2}^2\left(\Gamma_{12}+\Gamma_{14}\right)}{\beta\Gamma_{14}\left(T_{\mathrm{e}2}^2-d_{32}d_{42}\right)}+\frac{\mathrm{i}\Gamma_{12}d_{32}T_{\mathrm{e}2}^2}{\beta\Gamma_{14}},
\end{aligned}
$$

$$I_8 = -\frac{\mathrm{i}T_{\mathrm{e}1}^2 T_{\mathrm{e}2}^2 d_{32}^*}{\Gamma_{14}\left(T_{\mathrm{e}2}^2 - d_{32}^* d_{42}^*\right)\beta^*} + \frac{\mathrm{i}T_{\mathrm{e}2}^2 d_{32}^*}{\Gamma_{14}\beta^*} + \frac{\mathrm{i}d_{32}T_{\mathrm{e}1}^2 T_{\mathrm{e}2}^2}{\Gamma_{14}\left(T_{\mathrm{e}2}^2 - d_{32}d_{42}\right)\beta} - \frac{\mathrm{i}T_{\mathrm{e}2}^2 d_{32}}{\beta\Gamma_{14}}.$$

Acknowledgements

Project supported by the National Natural Science Foundation of China (Grant No. 51372214), Hunan Provincial Natural Science Foundation of China (Grant No. 2020JJ4240), and the Doctoral startup foundation of Hunan Institute of Engineering.

References

[1] Kimble H J 2008 *Nature* **453** 1023
[2] You Y, Lin G W, Feng L J, Niu Y P and Gong S Q 2021 *Chin. Phys. B* **30** 084207
[3] Fleischhauer M and Lukin M D 2000 *Phys. Rev. Lett.* **84** 5094
[4] Dinh X K, Nguyen H B, Nguyen L T A, Nguyen V P and Le V D 2022 *Chin. Phys. B* **31** 024201
[5] Jiang X J, Zhang H H and Wang Y Z 2016 *Chin. Phys. B* **25** 034204
[6] Wang D, Wu J Z and Zhang J X 2016 *Chin. Phys. B* **25** 064202
[7] Li Z D, Guo Q Q, Guo Y, He P B and Liu W M 2021 *Chin. Phys. B* **30** 107506
[8] Guo H, Qiu X, Ma Y, Jiang H F and Zhang X F 2021 *Chin. Phys. B* **30** 060310
[9] Li Z D, Wang Y Y and He P B 2019 *Chin. Phys. B* **28** 010504
[10] Sangouard N, Simon C, Riedmatten H D and Gisin N 2011 *Rev. Mod. Phys.* **83** 33
[11] Haus H A and Wong W S 1996 *Rev. Mod. Phys.* **68** 423
[12] Dong Y Y, Wang D L, Wang Y and Ding J W 2018 *Phys. Lett. A* **382** 2006
[13] Wu Y and Deng L 2004 *Phys. Rev. Lett.* **93** 143904
[14] Huang G X, Deng L and Payne M G 2005 *Phys. Rev. E* **72** 016617
[15] Wu Y and Deng L 2004 *Opt. Lett.* **29** 2064
[16] She Y C, Zhang W X and Wang D L 2011 *Acta. Phys. Sin.* **60** 064205 (in Chinese)
[17] Tan K B, Lu H M, Guan Q, Zhang G S and Chen C C 2018 *Acta Phys. Sin.* **67** 064207 (in Chinese)
[18] Zhao J D, Zhang H, Yang W G, Zhao J H, Jing M Y and Zhang L J 2021 *Acta Phys. Sin.* **70** 103201 (in Chinese)
[19] Chen Y, Bai Z Y and Huang G X 2014 *Phys. Rev. A* **89** 023835
[20] Bai Z Y, Hang C and Huang G X 2013 *Chin. Opt. Lett.* **11** 012701
[21] Chen Y, Chen Z M and Huang G X 2015 *Phys. Rev. A* **91** 023820
[22] Shou C and Huang G X 2019 *Phys. Rev. A* **99** 043821
[23] Chen Z M, Bai Z Y, Li H J, Hang C and Huang G X 2015 *Sci. Rep.* **5** 8211
[24] Simon C, Afzelius M, Appel J, Giroday A B, *et al.* 2010 *Eur. Phys. J. D* **58** 1
[25] Lodahl P, Mahmoodian S and Stobbe S 2015 *Rev. Mod. Phys.* **87** 347
[26] Mogilevtsev D, Reyes-Gomez E, Cavalcanti S B and Oliveira L E 2015 *Phys. Rev. B* **92** 235446
[27] Heshami K, England D G, Humphreys P C, Bustard P J, Acosta V M, Nunn J and Sussman B 2016 *J. Mod. Opt.* **63** 2005
[28] Hepp S, Jetter M, Portalupi S L and Michler P 2019 *Adv. Quantum Technol.* **2** 1900020
[29] Hamedi H R 2016 *J. Opt. Soc. Am. B* **33** 151
[30] Giroday A B, Skold N, Stevenson R M, Farrer I, Ritchie D A and Shields A J 2011 *Phys. Rev. Lett.* **106** 216802
[31] Tang H, Wang D L, Zhang W X, Ding J W and Xiao S G 2017 *Acta. Phys. Sin.* **66** 034202 (in Chinese)
[32] Yang X, Wang Y, Wang D L and Ding J W 2020 *Acta Phys. Sin.* **69** 174203 (in Chinese)
[33] Zeng K H, Wang D L, She Y C and Zhang W X 2013 *Acta. Phys. Sin.* **62** 147801 (in Chinese)
[34] Yuan C H and Zhu K D 2006 *Appl. Phys. Lett.* **89** 052115
[35] Borges H S, Sanz L, Villas-Boas J M, Neto O O D and Alcalde A M 2012 *Phys. Rev. B* **85** 115425
[36] Sun D, Zhang H J, Sun H, Li X W and Wang G Y 2019 *Phys. Lett. A* **383** 148
[37] Li J, Liu J and Yang X 2008 *Physica E* **40** 2916
[38] She Y C, Zheng X J, Wang D L and Zhang W X 2013 *Opt. Express* **21** 17392
[39] Beirne G J, Hermannstadter C, Wang L, Rastelli A, Schmidt O G and Michler P 2006 *Phys. Rev. Lett.* **96** 137401
[40] Gaudreau L, Studenikin S A, Sachrajda A S, Zawadzki P, Kam A, Lapointe J, Korkusinski M and Hawrylak P 2006 *Phys. Rev. Lett.* **97** 036807
[41] Hsieh C Y, Shim Y P, Korkusinski M and Hawrylak P 2012 *Rep. Prog. Phys.* **75** 114501
[42] Wang L, Rastelli A, Kiravittaya S, Benyoucef M and Schmidt O G 2009 *Adv. Mater.* **21** 2601
[43] Tian S C, Wan R G, Tong C Z, Ning Y Q, Qin L and Liu Y 2014 *J. Opt. Soc. Am. B* **31** 1436
[44] Tian S C, Wan R G, Tong C Z, Fu X H, Cao J S and Ning Y Q 2015 *Laser Phys. Lett.* **12** 125203
[45] Luo X Q, Li Z Z, Jing J, Xiong W, Li T F and Yu T 2018 *Sci. Rep.* **8** 3107
[46] Luo X Q, Li Z Z, Li T F, Xiong W and You J Q 2018 *Opt. Express* **26** 32585
[47] Wang Y, Ding J W and Wang D L 2020 *Eur. Phys. J. D* **74** 190
[48] Lvovsky A I, Sanders B C and Tittel W 2009 *Nat. Photonics* **3** 706
[49] Ma L, Slattery O and Tang X 2017 *J. Opt.* **19** 043001
[50] Bracker A S, Scheibner M, Doty M F, Stinaff E A, Ponomarev I V, Kim J C, Whitman L J, Reinecke T L and Gammon D 2006 *Appl. Phys. Lett.* **89** 233110
[51] Borges H S, Sanz L, Villas-Boas J M and Alcalde A M 2013 *Appl. Phys. Lett.* **103** 222101
[52] Li H J and Huang G X 2008 *Phys. Lett. A* **372** 4127
[53] Such a detaled theoretical explanation, refer to Fig. 4 of Ref. [19].